Clathrate Ba_6Ge_{25}: Thermodynamic, magnetic, and transport properties

S. Paschen, V. H. Tran,* M. Baenitz, W. Carrillo-Cabrera, Yu. Grin, and F. Steglich
Max Planck Institute for Chemical Physics of Solids, Nöthnitzer Str. 40, D - 01187 Dresden, Germany
(Received 30 November 2001; published 26 March 2002)

The recently discovered clathrate Ba_6Ge_{25} undergoes a two-step first-order phase transition at the temperatures $T_{S1,S2} \approx 215$, 180 K. The first-order nature of the transition is evidenced from the hysteretical temperature dependences of the electrical resistivity $\rho(T)$, the Hall coefficient $R_H(T)$, and the magnetic susceptibility as well as from the temperature dependence of the specific heat. $\rho(T)$ increases drastically below $T_{S1,S2}$, but the charge-carrier concentration, as determined from $R_H(T)$, is virtually unaffected by the phase transition. Thus, it is the charge-carrier mobility which is strongly reduced below $T_{S1,S2}$. Taking these observations together with results from a recent structural investigation we conclude that the ''locking-in'' of ''rattling'' Ba atoms to off-center positions in the Ge cages is responsible for the mobility reduction of the conduction electrons. It is due to this strong electron-phonon interaction that, while the concept of a ''phonon glass'' appears to be fulfilled, the concept of an ''electron crystal'' is heavily violated, in contrast to other filled-cage systems. In the phase $Ba_{6-x}Eu_xGe_{25}$ ($x \leqslant 0.6$), $T_{S1,S2}$ is quickly suppressed with increasing x and, in $Ba_4Na_2Ge_{25}$ [$Ba_{6-x}Na_xGe_{25}$ ($x=2$)], the locking-in transition is absent alltogether at temperatures below 400 K.

DOI: 10.1103/PhysRevB.65.134435 PACS number(s): 75.20.−g, 72.15.Jf, 61.48.+c

I. INTRODUCTION

The clathrate Ba_6Ge_{25} was discovered by Carrillo-Cabrera *et al.*[1,2] Very recently, two other groups confirmed the existence of this compound.[3,4] Ba_6Ge_{25} belongs to the structure family of chiral clathrates $cP124$ and is a binary variant of the $Ba_6In_4Ge_{21}$ type.[5] Ba_6Ge_{25} is cubic with the room-temperature lattice parameter $a=14.5564(2)$ Å. Each unit cell contains four Ba_6Ge_{25} formula units. There are three different lattice sites for the Ba atoms in the structure. The atoms of the Ba1 site occupy the Ge_{20} polyhedra and the two remaining Ba sites (Ba2 and Ba3) are located in the cavities of the zeolitelike labyrinth created by the nonspace-filling three-dimensional arrangement of the Ge_{20} polyhedra. There are two Ba1 atoms, three Ba2 atoms, and one Ba3 atom per Ba_6Ge_{25} formula unit. The structure contains both threefold bonded ($3b$) and fourfold bonded ($4b$) Ge atoms. In terms of the Zintl concept,[6] Ba_6Ge_{25} may be written as $(Ba^{2+})_6((3b)Ge^{1-})_8((4b)Ge^0)_{17}(4e^-)$.[1,2] Thus, four conduction electrons are expected per Ba_6Ge_{25} unit, corresponding to a relatively small charge-carrier concentration of approximately 5×10^{21} cm^{-3}. $Ba_4Na_2Ge_{25}$ [$Ba_{6-x}Na_xGe_{25}$ ($x=2$)] is isostructural to Ba_6Ge_{25}, with the room-temperature lattice parameter $a=14.4703(2)$ Å.[7] The two Na atoms per $Ba_4Na_2Ge_{25}$ formula unit occupy part of the Ba2 sites (in a ratio Na:Ba = 2:1). The Zintl electron count $(Ba^{2+})_4(Na^{1+})_2((3b)Ge^{1-})_8((4b)Ge^0)_{17}(2e^-)$ yields two conduction electrons per $Ba_4Na_2Ge_{25}$ formula unit. Ba_6Ge_{25} may also be doped with Eu.[8] The Ba atoms at both the Ba1 and the Ba3 sites are partially replaced by Eu, but no Eu is found on the Ba2 site. The maximum solubility is about 10%, or $x=0.6$ in $Ba_{6-x}Eu_xGe_{25}$. For $x \leqslant 0.6$, the room-temperature lattice parameter decreases linearly with increasing Eu content until $a=14.5271(2)$ Å.[8]

The large room-temperature values of the atomic displacement factors for the Ba2 and Ba3 sites in Ba_6Ge_{25}, as determined from x-ray diffraction studies, give evidence for the Ba atoms ''rattling'' at these two sites.[1,2] In a recent structural study[8] it was shown that, upon cooling, these atomic displacement factors increase strongly in the temperature range of the phase transition. This is interpreted as being due to the Ba atoms ''locking-in'' to well-separated positions (split sites), which were labeled Ba4 for the Ba2 site and Ba3′ for the Ba3 site. The Ba3 atoms seem to lock in at a slightly higher temperature than the Ba2 atoms. Since no superstructure could be resolved below the phase-transition temperature, we believe that the split sites are occupied randomly.

The renewed interest in clathrates[9–12] stems from the claim[13] that they behave as ''phonon glasses'' and ''electron crystals'' and, therefore, are promising thermoelectric materials. Atoms located in oversized atomic cages are believed to undergo large local vibrations, somewhat independent of the other atoms in the crystal. This rattling may lead to very low and glasslike lattice thermal conductivities κ (phonon glasses). Supposing that κ is phonon dominated, the rattling will increase the thermoelectric figure of merit $Z=S^2\sigma/\kappa$ only if it affects the conduction electrons, and therefore also the electrical conductivity σ, much less than the phonons. In this case the electrons behave as electrons in a crystalline lattice (electron crystals). This assumes that the lattice degrees of freedom related to the rattling are essentially decoupled from the electronic degrees of freedom. As we shall show below, this is not the case for Ba_6Ge_{25}. Here, the reduction of the rattling due to the locking-in of the Ba atoms below the phase-transition temperature goes hand in hand with a pronounced reduction of the charge-carrier mobility.

II. EXPERIMENTAL SETUP

The preparation and structural characterization of the polycrystalline Ba_6Ge_{25}, $Ba_{6-x}Eu_xGe_{25}$, and $Ba_4Na_2Ge_{25}$ samples investigated here is described elsewhere.[1,2,7,8,14] The magnetic susceptibility was measured between 2 and 400 K using a superconducting quantum interference device mag-

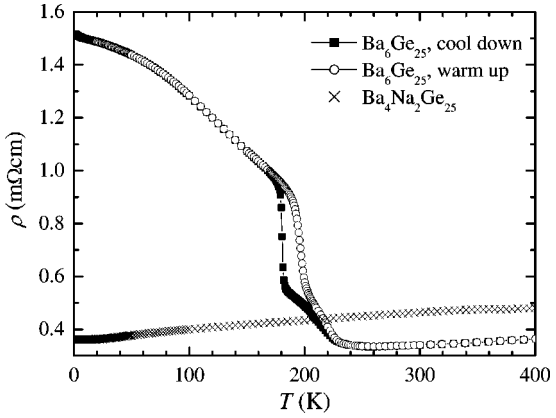

FIG. 1. Electrical resistivity ρ of Ba_6Ge_{25} and $Ba_4Na_2Ge_{25}$ as a function of temperature T.

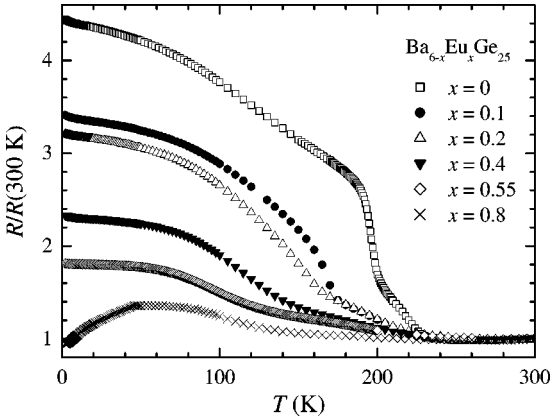

FIG. 2. Electrical resistance taken during warm-up sweep, normalized to its value at 300 K, $R/R(300\ \mathrm{K})$ of $Ba_{6-x}Eu_xGe_{25}$ as a function of temperature T.

netometer. Except below 50 K, the susceptibility is field independent up to at least 5 T. The specific heat was determined with a relaxation-type method between 2 and 300 K. ac measurements of the electrical resistivity and the Hall coefficient were performed between 2 and 400 K in magnetic fields up to 13 T. For the Hall-effect measurements a standard setup with the two Hall-voltage contacts perpendicular to the directions of the electrical current and of the magnetic field was used. In order to eliminate the misalignment voltage, the sample was, at each field and temperature setting, first measured in an upright position, then turned by 180°, and subsequently measured in a downward position. The thermal conductivity and the thermopower were measured with a steady-state method between 5 and 150 K and between 2 and 300 K, respectively.

III. EXPERIMENTAL RESULTS AND ANALYSIS

In Fig. 1 we show the temperature dependence of the electrical resistivity $\rho(T)$ of Ba_6Ge_{25}. Between 400 and 260 K, ρ decreases with decreasing T, a sign of metallic conduction. Between 230 and 170 K, ρ increases steeply. The increase occurs in two steps. The warming-up $\rho(T)$ curve is distinctly different from the cooling-down curve in this temperature range. Such a thermal hysteresis effect is typical for first-order phase transitions. The temperatures of the two steps, $T_{S1,S2}\approx 215$, 180 K, are determined as the average of the cooling-down and warming-up temperatures where $|d\rho/dT|$ assumes a maximum. Below 170 K, ρ continues to increase with decreasing T. For comparison, we also plot $\rho(T)$ of $Ba_4Na_2Ge_{25}$ in Fig. 1. Starting from similar resistivity values at 400 K, $\rho(T)$ of $Ba_4Na_2Ge_{25}$ does not show the anomalous increase observed for Ba_6Ge_{25}, but follows a simple metal-like temperature dependence in the entire temperature range.

Figure 2 shows the temperature dependence of the electrical resistance normalized to its room-temperature value $R/R(300\ \mathrm{K})(T)$ of a series of Eu-doped samples of the composition $Ba_{6-x}Eu_xGe_{25}$ with $x\leqslant 0.8$. Except for the sample with $x=0.8$, all samples were shown to be single phase.[8] All curves were taken during warm-up sweeps. Already small amounts of doping lower the phase-transition temperature $T_{S1,S2}$ considerably and broaden the temperature range of the transition.

To disentangle the effect of charge-carrier concentration n and mobility μ on the electrical conductivity which, for a simple parabolic band is $\sigma=ne\mu$, Hall-effect measurements were performed. In Fig. 3 we show the temperature dependence of the effective charge-carrier concentration $n(T)$ determined from the Hall coefficient $R_H(T)$ by assuming a one-band model, i.e., $n=1/(R_He)$.[15] This simple approach is justified by the fact that the Hall resistivity $\rho_H=R_HB$ is, in the entire temperature range, a linear function of the applied magnetic field H. Typical isothermal ρ_H vs $B=\mu_0H$ curves are shown in Fig. 4. n is negative in the entire temperature range between 2 and 400 K, indicating that the charge carriers are electron like. At 2 K, n corresponds to approximately 6 electrons per Ba_6Ge_{25} formula unit (7.8×10^{21} cm^{-3}), in relatively good agreement with the 4 electrons per Ba_6Ge_{25} formula unit expecteded from the Zintl rule. Upon increasing the temperature, the charge-carrier concentration increases smoothly and reaches 13 electrons per Ba_6Ge_{25} formula unit (1.7×10^{22} cm^{-3}) at 400 K. The anomalies in the temperature range of the phase transition, which are different for the cooling-down and warming-up curves, are most probably related to the nonequilibrium conditions. Most important, how-

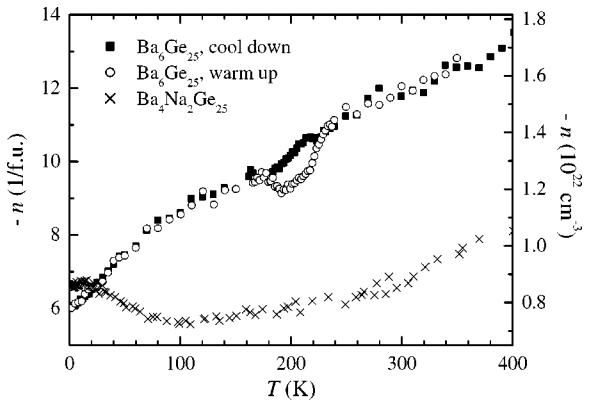

FIG. 3. Temperature dependence of the (negative) charge-carrier concentration $-n(T)$ of Ba_6Ge_{25} and of $Ba_4Na_2Ge_{25}$.

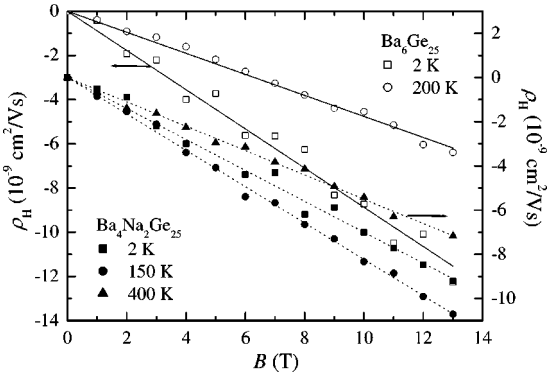

FIG. 4. Hall resistivity ρ_H vs magnetic field $B=\mu_0 H$ at 2 and 200 K for Ba_6Ge_{25} and at 2, 150, and 400 K for $Ba_4Na_2Ge_{25}$. The lines are best linear fits to the data.

ever, is that we do not observe a pronounced change in $n(T)$ at the temperature of the phase transition; i.e., the charge-carrier concentration is virtually unaffected by the phase transition. Thus, a change of the mobility must be responsible for the strong change of the resistivity. As may be seen in Fig. 5, this is indeed the case: The temperature dependence of the absolute value of the Hall mobility $|\mu_H|(T) = |R_H|(T)/\rho(T)$, plotted as data points, closely resembles the $\sigma(T)=1/\rho(T)$ data, plotted as solid and dotted curves, at least between 100 and 240 K. At 2 K, $|\mu_H|(T)$ is, with 0.6 $cm^2/V\,s$, extremely small. This is also reflected in a very short mean free path (inset of Fig. 5), estimated from the free-electron formula $l=h/(2\rho)\times[3R_H^2/(\pi e^4)]^{1/3}$ to be only 2.4 Å at 2 K. For comparison we have also measured the Hall coefficient of $Ba_4Na_2Ge_{25}$. The charge-carrier concentration (Fig. 3), again determined in a one-band model, varies less with temperature than $n(T)$ of Ba_6Ge_{25}. At 2 K it is, with 6.6 electrons per $Ba_4Na_2Ge_{25}$ formula unit (8.7×10^{21} cm^{-3}), slightly larger than for Ba_6Ge_{25}. This is in contrast to the Zintl rule which predicts, with 2 electrons per $Ba_4Na_2Ge_{25}$ formula unit, a lower charge-carrier concentration for $Ba_4Na_2Ge_{25}$ than for Ba_6Ge_{25}. The one-band analysis of the R_H data of $Ba_4Na_2Ge_{25}$ is again supported by linear $\rho_H(B)$ curves (Fig. 4). $|\mu_H|(T)$ is distinctly larger for $Ba_4Na_2Ge_{25}$ than for Ba_6Ge_{25}, especially at low temperatures. At 2 K, $|\mu_H|$ of $Ba_4Na_2Ge_{25}$ is, with 2 $cm^2/V\,s$, more than a factor of 3 larger than $|\mu_H|$ of Ba_6Ge_{25} (Fig. 6). The mean free path of $Ba_4Na_2Ge_{25}$ is shown in the inset of Fig. 6.

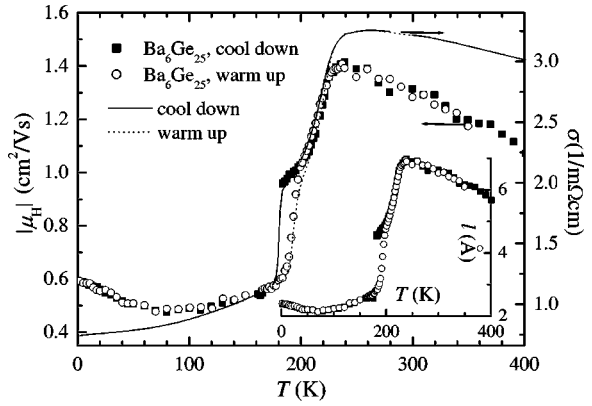

FIG. 5. Absolute value of the Hall mobility $|\mu_H|$ (open and solid symbols, left scale) and of the electrical conductivity σ (solid and dotted curves, right scale) for Ba_6Ge_{25} as a function of temperature T. The inset shows the temperature dependence of the mean free path $l(T)$ for Ba_6Ge_{25}, supposing that the effective mass of the charge carriers is equal to the free-electron mass.

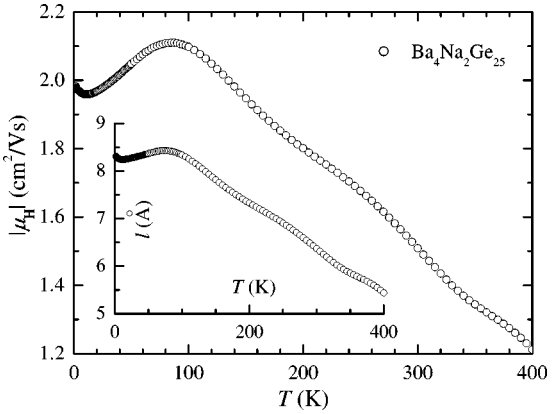

FIG. 6. Absolute value of the Hall mobility $|\mu_H|$ as a function of temperature T for $Ba_4Na_2Ge_{25}$. The inset shows the temperature dependence of the mean free path $l(T)$ for $Ba_4Na_2Ge_{25}$, supposing that the effective mass of the charge carriers is equal to the free-electron mass.

In Fig. 7 several isothermal magnetoresistance (MR) versus applied magnetic field curves, $MR(B)=[R(B)-R(0)]/R(0)$, where R is the electrical resistance, are shown for Ba_6Ge_{25} and $Ba_4Na_2Ge_{25}$. MR is relatively small and positive in the entire temperature range. At 2 K and 13 T, MR reaches 0.7% and 1.6% for Ba_6Ge_{25} and $Ba_4Na_2Ge_{25}$, respectively. Such a MR behavior is in qualitative agreement with the predictions for the MR due to weak localization effects.[16]

The magnetic susceptibility $\chi(T)$ of Ba_6Ge_{25}, measured in a magnetic field of 5 T, is plotted in Fig. 8. It is negative between 2 and 400 K which may be attributed to a predominant Larmor diamagnetic susceptibility of filled electronic shells, χ_{Larmor}. A rough estimate of χ_{Larmor} using tabulated

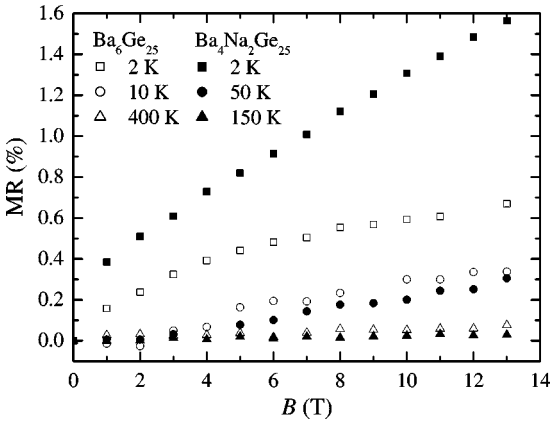

FIG. 7. Magnetoresistance MR as a function of temperature T for Ba_6Ge_{25} and for $Ba_4Na_2Ge_{25}$.

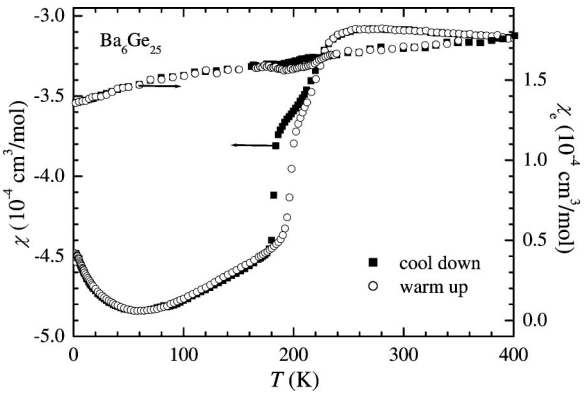

FIG. 8. Temperature dependence of the total magnetic susceptibility $\chi(T)$ for Ba_6Ge_{25} in a magnetic field of 5 T (left scale) and of the electronic part $\chi_e(T)$ (right scale) as estimated from the Hall-effect data using a free-electron model.

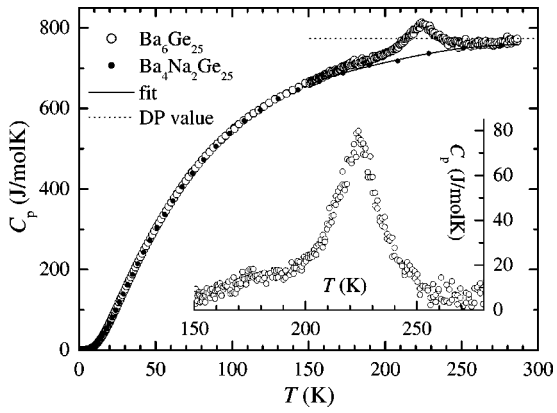

FIG. 9. Specific heat C_p as a function of temperature T for Ba_6Ge_{25} and for $Ba_4Na_2Ge_{25}$. The dotted line denotes the Dulong-Petit (DP) value. The inset shows an enlarged view of the specific heat of Ba_6Ge_{25} after subtracting the fit (solid curve) to the specific heat of $Ba_4Na_2Ge_{25}$, which serves as a ''phase-transition-free'' phonon background.

values for closed-shell cations[17] gives -3.7×10^{-4} cm^3/mol for Ba_6Ge_{25}. The measured susceptibility of Ba_6Ge_{25} varies between -4.8×10^{-4} cm^3/mol at 55 K and -3.1×10^{-4} cm^3/mol at 260 K. It has been suggested[18] that in clathrates there is an additional diamagnetic contribution, the so-called structural increment χ_{struct}, which accounts for molecular ring currents induced by the Lorentz force in a magnetic field. In both graphite and C_{60}, electron orbits circulating round the plane hexagonal rings of carbon give rise to such diamagnetic ring currents.[19] The low-temperature susceptibility of Ba_6Ge_{25} being larger in absolute value than χ_{Larmor} may be due to this effect. Upon cooling down, χ decreases first gradually below 260 K and then very sharply between 185 and 175 K. Again, the transition is two-step like and is accompanied by a thermal hysteresis. The low-temperature upturn is strongly field dependent. The magnetization versus field curve $M(B)$ at 2 K may be decomposed into a linear-in-B diamagnetic contribution and a paramagnetic contribution χ_{para} with a saturation magnetization of 6×10^{-4} μ_B/f.u. This latter contribution is most probably due to a very small amount of magnetic impurities. Also plotted in Fig. 8 is the conduction-electron contribution $\chi_e(T)$ as estimated in a free-electron model from the charge-carrier concentration obtained from the Hall-effect measurement. χ_e contains the Pauli paramagnetism and the Landau diamagnetism of the conduction electrons, assuming that the effective mass of the electrons is the free-electron mass. From a comparison of the measured susceptibility $\chi(T)$ with $\chi_e(T)$ it is obvious that the strong decrease of $\chi(T)$ upon cooling below the phase-transition temperature cannot be due to the slight and smooth decrease of $\chi_e(T)$. Surprisingly, $\chi(T)$ decreases by approximately 1.8×10^{-4} cm^3/mol between 270 and 60 K, which is close to the value of $\chi_e(T)$ at 400 K.

The temperature dependence of the specific heat $C_p(T)$ of Ba_6Ge_{25} is shown in Fig. 9. Between 190 and 260 K, a pronounced symmetric anomaly with a maximum at 223 K is identified, indicating a first-order phase transition at this latter temperature. A much smaller second anomaly may be identified at approximately 185 K. The temperatures of these anomalies being higher than $T_{S1,S2}$ determined above from the $\rho(T)$ data is most probably due to the fact that $C_p(T)$ was measured during a warm-up sweep. Also plotted in Fig. 9 is the specific heat of $Ba_4Na_2Ge_{25}$. In the investigated temperature range, $C_p(T)$ is smooth, with no sign of a phase transition. Away from the anomalies of Ba_6Ge_{25}, both $C_p(T)$ curves ressemble each other closely, especially at temperatures above 10 K. Thus, in the temperature range of the phase transition, $C_p(T)$ of $Ba_4Na_2Ge_{25}$ may be taken as a ''phase-transition-free'' phononic background for Ba_6Ge_{25}. The difference between the Ba_6Ge_{25} and the $Ba_4Na_2Ge_{25}$ data is plotted in the inset of Fig. 9. Here, the second anomaly at approximately 185 K is seen more clearly. The entropy per mole Ba_6Ge_{25} of both anomalies is $1.47R$, where R is the gas constant. This is an unusually large entropy release for a structural (first-order) phase transition which may indicate that a second-order phase transition goes hand in hand with the structural transition. The electronic contribution to the specific heat $C_e(T)=\gamma T$ was determined for both Ba_6Ge_{25} and $Ba_4Na_2Ge_{25}$ at very low temperatures[20] from the intercepts of $C_p/T=\gamma+\beta T^2$ fits. The second term corresponds to the low-temperature phononic contribution. $\beta=3.8$ mJ/mol K^2 was found for both compounds, corresponding to a Debye temperature $\Theta_D=250$ K. The values obtained for γ were 21 mJ/mol K^2 for Ba_6Ge_{25} and 33 mJ/mol K^2 for $Ba_4Na_2Ge_{25}$. Combining these values with the charge-carrier concentrations extracted from the Hall coefficients discussed above by using a simple free-electron model, i.e., $\gamma=k_B^2 m(3\pi^2 n)^{1/3}/(3\hbar^2)$, we obtain effective masses m of $1.4m_0$ and $2.2m_0$ for Ba_6Ge_{25} and $Ba_4Na_2Ge_{25}$, respectively, where m_0 is the free-electron mass. At 300 K, the Dulong-Petit value of 773 J/mol K ($=3R\times31$ atoms of the formula unit), shown as a dotted line in Fig. 9, is almost reached.

The thermoelectric power $S(T)$ of Ba_6Ge_{25}, displayed in Fig. 10, is negative between 2 and 300 K, in agreement with the negative Hall coefficient. At room temperature, S reaches a moderate value of -20 μV/K. Between 230 and 300 K, S

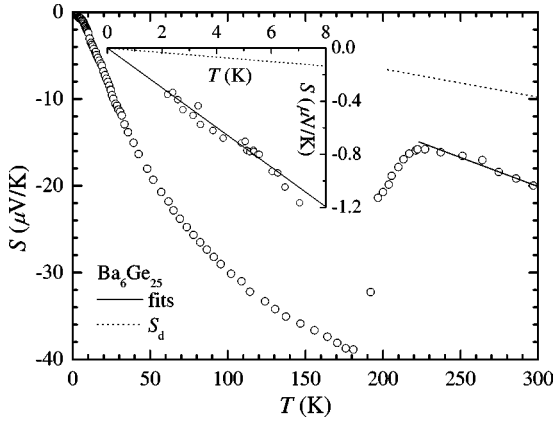

FIG. 10. Thermopower S as a function of temperature T for Ba_6Ge_{25}. The inset shows a close up of the low-temperature data. The solid lines are best linear fits to the data at $T>230$ K and at $T<6.5$ K (inset). The dotted lines denote the high- and low-temperature (inset) limit of the diffusion thermopower S_d, estimated as explained in the text.

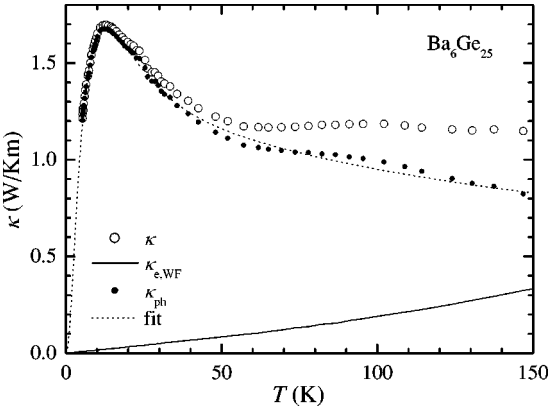

FIG. 11. Total measured thermal conductivity κ, its electronic contribution $\kappa_{e,WF}$, as estimated from the electrical resistivity using the Wiedemann-Franz law, its phonon contribution $\kappa_{ph}=\kappa-\kappa_{e,WF}$, and the fit to κ_{ph} as discssed in the text, as a function of temperature T for Ba_6Ge_{25}.

varies approximately linearly with T. Such a variation is expected for the diffusion thermopower in the free-electron approximation above the Debye temperature Θ_D where electron-phonon scattering is the dominant scattering mechanism, which is $S_d(T>\Theta_D)=\pi^2k_B^2 2m/[e\hbar^2(3n\pi^2)^{2/3}]\times T$. Also at the lowest temperatures (below 6.5 K), a linear $S(T)$ behavior is found (cf. inset of Fig. 10), consistent with the diffusion thermopower of a simple metal in the residual resistance region, which is $S_d(T\ll\Theta_D)=1/3\times S_d(T>\Theta_D)$. Using the charge-carrier concentrations extracted from the Hall coefficient at 300 K and at 2 K, S_d according to these two relations is plotted in Fig. 10 as dotted lines. The slopes of these lines are smaller than the slopes of the linear fits to the experimental data (solid lines), suggesting that the effective masses of the charge carriers are enhanced. Agreement between theoretical and experimental curves would be obtained for $m=9m_0$ at low and $m=2m_0$ at high temperatures. Upon cooling below 220 K, the absolute value of S increases anomalously. This is most probably related to the phase transition and may reflect a modification of the Fermi surface associated with the phase transition, consistent with a change of the effective mass.

The temperature dependence of the thermal conductivity $\kappa(T)$ of Ba_6Ge_{25} between 5 and 150 K is presented in Fig. 11. At 150 K, the electronic contribution $\kappa_{e,WF}$, estimated from the electrical resistivity $\rho(T)$ measured on the same sample by using the Wiedemann-Franz law $\kappa_e(T)=\pi^2k_B^2/(3e^2)\times T/\rho(T)$, is approximately 30% of the measured total thermal conductivity $\kappa=\kappa_{e,WF}+\kappa_{ph}$. Preliminary results confirm, however, the observation reported in Ref. 4 that, at room temperature, κ is dominated by the electronic contribution. At the lowest temperatures the phonon contribution κ_{ph} dominates, $\kappa_{e,WF}$ falling below 1% of κ at 10 K. At 13 K, the thermal conductivity displays a maximum. However, this maximum is much less pronounced than the maxima due to phonon umklapp scattering usually observed in pure crystalline materials. In particular, the increase of κ upon cooling below 60 K is much weaker than the $1/T$ or $\exp(1/aT)$ laws expected for umklapp scattering. Thus, the thermal conductivity of Ba_6Ge_{25} clearly reveals the presence of some sort of disorder in the system.

Similar observations made in other clathrates are discussed in a number of publications.[21] The essence is that the heat-carrying acoustic phonons, which are framework derived, are assumed to be strongly scattered from the local vibrations of the guest atoms, leading to a dip in the thermal conductivity in the temperature range 4–35 K. For Ba_6Ge_{25}, such a dip occurs at a somewhat higher temperature of approximately 50 K. In Refs. 22 and 23, $\kappa_{ph}(T)$ of the clathrate $Eu_8Ga_{16}Ge_{30}$ was fitted by a phenomenological model put forward by Cohn *et al.*[24] In this model, $\kappa_{ph}(T)$ is calculated from the kinetic-gas-theory expression $\kappa_{ph}=(v/3)\int_0^{\omega_D}C(\omega)l(\omega)d\omega$ with a Debye specific heat C and, assuming the validity of Matthiessen's rule, a phonon mean free path l that is the sum of terms representing tunneling states (TS's), resonant scattering (res), and Rayleigh (R) scattering: $l=(l_{TS}^{-1}+l_{res}^{-1}+l_R^{-1})^{-1}+l_{min}$, with $l_{TS}^{-1}=A(\hbar\omega/k_B)\tanh(\hbar\omega/2k_BT)+(A/2)(k_B/\hbar\omega+B^{-1}T^{-3})^{-1}$, $l_{res}^{-1}=\Sigma_{i=1}^{2}N_i\omega^2T^2/[(\omega_i^2-\omega^2)^2+\gamma_i\omega_i^2\omega^2]$, and $l_R^{-1}=D(\hbar\omega/k_B)^4$. The lower limit on l was assumed to be a constant, l_{min}. Thus, this model takes, in addition to mass-density scattering (R), two scattering mechanisms related to the filled-cage structure into account: The resonant scattering (res) is directly related to the rattling of the guest atoms in the oversized cages and the scattering from tunneling states (TS's) may be associated with guest atoms tunneling between different split sites.

The local vibrations of the guest atoms are also expected to strongly influence the specific heat, contributing as low-energy Einstein modes. Thus, the lattice contribution to the specific heat of Ba_6Ge_{25} should be modeled by the sum of a Debye term (from all Ge atoms) and one or more Einstein terms (from the Ba atoms).

Our analysis of the $\kappa_{ph}(T)$ and $C_{ph}(T)$ data reveals that two different Einstein frequencies are sufficient to obtain good fits. In a first step we fitted both $\kappa_{ph}(T)$ and $C_{ph}(T)$ in the same run letting all fit parameters adjust freely. For the

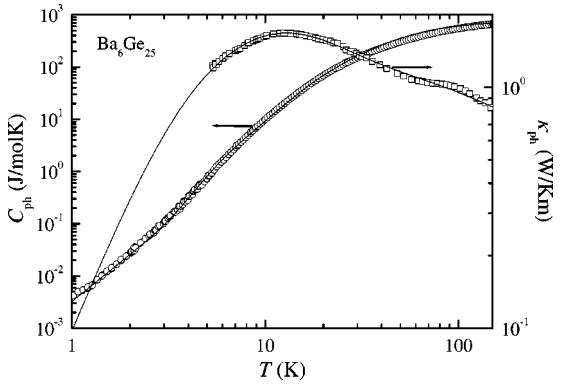

FIG. 12. Phonon contributions to the specific heat C_{ph} and to the thermal conductivity κ_{ph} as a function of temperature T for Ba_6Ge_{25}. The solid curves correspond to the fits discussed in the text.

ratio N_1/N_2, which corresponds to the ratio of the number of guest atoms oscillating with frequencies corresponding to the Einstein temperatures Θ_{E1} and Θ_{E2}, we obtained 11; i.e., per Ba_6Ge_{25} formula unit there would be only 0.5 Ba atoms with the Einstein temperature Θ_{E2} (and 5.5 Ba atoms with Θ_{E1}). Since a noninteger number of Ba atoms is an unphysical result, we fixed, in a second step, the ratio N_1/N_2 to 5, i.e., to 1 Ba atom per Ba_6Ge_{25} formula unit with the Einstein temperature Θ_{E2} (and 5 Ba atoms with Θ_{E1}). All other fit parameters were left open. A fit (cf. dotted curve in Fig. 11 and solid curves in Fig. 12) of very similar quality to the first one was obtained and the fitted values of all parameters were within 25% of the values obtained in the first fit. We obtain $\Theta_D = 240$ K [corresponding to the sound velocity $v = (\Theta_D k_B/\hbar)/(6\pi^2 n)^{1/3} = 2350$ m/s, where n is the number of atoms per unit volume], $l_{min} = 2.2$ Å, $A = 2.7\times10^4$ m^{-1} K^{-1}, $B = 3.0\times10^{-2}$ K^{-2}, $N_1 = 4.7\times10^{30}$ m^{-1} s^{-2} K^{-2}, $N_2 = 9.4\times10^{29}$ m^{-1} s^{-2} K^{-2}, $\gamma_1 = 4.1$, $\gamma_2 = 3.5$, $D = 4.1$ m^{-1} K^{-4}, $\Theta_{E1} = 104$ K, and $\Theta_{E2} = 44$ K. The ratio A/B, a measure of the density of strongly coupled tunneling states,[22] is larger than the one found for the α modification but smaller than the one found for the β modification of $Eu_8Ga_{16}Ge_{30}$ in Ref. 23. While in α-$Eu_8Ga_{16}Ge_{30}$ there exist no split sites, in both Ba_6Ge_{25} and β-$Eu_8Ga_{16}Ge_{30}$ split sites are needed to understand the x-ray data.[8,23] Thus, the tunneling between the split sites seems to be less efficient in Ba_6Ge_{25} than in β-$Eu_8Ga_{16}Ge_{30}$, probably due to the very large split-site separations in the former compound. The larger value of D for Ba_6Ge_{25} than for both α- and β-$Eu_8Ga_{16}Ge_{30}$ indicates greater mass density variations in the first compound. It should be mentioned that the lower limit on the phonon mean free path l_{min} is in excellent agreement with the electronic mean free path at low temperatures (cf. Fig. 5), indicating that phonons and electrons are closely related to each other in Ba_6Ge_{25}.

The dimensionless thermoelectric figure of merit ZT of Ba_6Ge_{25} increases monotonically with temperature and reaches a value of 0.015 at 150 K. Below 100 K, our thermal-conductivity data are in good overall agreement with those of Ref. 4. Assuming that this holds true up to at least 180 K, ZT of the sample investigated here reaches a maximum value of 0.05 at 180 K. This value is comparable to ZT of $Eu_8Ga_{16}Ge_{30}$ at the same temperature.[23]

A comparison of the electrical resistivity and the thermopower data presented in Ref. 4 with our data reveals several discrepancies. The room-temperature resistivity value of our samples is, with 340 $\mu\Omega$ cm, distinctly lower than the 500 $\mu\Omega$ cm given in Ref. 4. In addition, our resistivity data have a much richer temperature dependence, with the strong variation in the temperature range of the phase transition and the pronounced hysteresis effect discussed above. In the resistivity data of Ref. 4 there is no clear indication of a phase transition. Only a small kink in the temperature dependence of the thermopower shown in Ref. 4 might be a sign of the transition. The kink is more pronounced in our data and the absolute values of the thermopower are about a factor of 2 larger for our samples than for those studied in Ref. 4.

IV. DISCUSSION

We put the main emphasis in this study on the understanding of the relation between structural and electronic properties of Ba_6Ge_{25} and on how they are modified in the course of the observed first-order phase transition at $T_{S1,S2}$. In other words, what happens at the phase transition? How are the changes in the electronic properties related to the structural changes?

Let us first summarize the most important experimental findings. Upon cooling below $T_{S1,S2}$, the electrical resistivity increases steeply while the Hall coefficient remains virtually unchanged. The magnetic susceptibility decreases steeply and the absolute value of the thermopower is strongly enhanced.

In a first approach we shall argue within the free-electron approximation; i.e., we neglect any real band structure effects and assume parabolic bands instead. In this picture the combination of the Hall-coefficient and magnetic-susceptibility data poses a puzzle. As shown in the previous section, the magnetic susceptibility χ decreases steeply at $T_{S1,S2}$ by approximately the conduction-electron contribution χ_e (derived from the Hall-coefficient data) while the charge-carrier concentration itself is virtually unaffected. This suggests that even though the conduction electrons are not lost as charge carriers during the phase transition, they *are* lost as spin carriers. Thus the conduction-electron spins have to be compensated by some means, for example, by the formation of spin-singlet pairs. It is known that such spin-singlet pairs are stable in a number of compounds with large electron-phonon coupling, where two conduction electrons together with a lattice deformation build a spinless bipolaron.[25] The formation of polaronic quasiparticles below $T_{S1,S2}$ is particularly appealing in view of the strong reduction of the Hall mobility below $T_{S1,S2}$. Also the increase of the effective mass of the charge carriers, suggested by the above analysis of the thermopower data in terms of the diffusion thermopower, supports this picture. The observed mobilities of the order of 1 cm^2/V s (cf. Fig. 5) are at the border between those typical for large and those typical for small (bi)polarons.[26] However, since no hopping transport[27] is observed at low temperatures,

the bipolarons in Ba_6Ge_{25} seem to be large[28] and give rise to bandlike transport. Also the temperature dependence of the mobility which, between 25 and 80 K, is inversely proportional to the temperature is in agreement with the predictions for large bipolarons.[28] According to an x-ray investigation,[8] the locking-in process results in short Ba3′-Ba4 distances: at 10 K the shortest Ba3′-Ba4 distance is 4.03 Å. In undistorted Ba_6Ge_{25}, Ba3 has six nearest-neighbor Ba2 atoms at a distance of 4.63 Å at 300 K.[8] From this we propose a microscopic picture for the bipolarons: Each short Ba3′-Ba4 distance is dynamically stabilized by two electrons forming a bipolaron. In order to compensate all conduction electron spins, all six conduction electrons present at 2 K (cf. Fig. 3) have to form bipolarons. Thus, three short Ba3′-Ba4 distances per Ba_6Ge_{25} formula unit would be needed. The electrons forming the bipolarons are most probably concentrated on that part of the Ge-cage surface which lies inbetween the Ba3′ and the Ba4 atoms. We should mention that the exceptionally large displaceability of the Ba ions in Ba_6Ge_{25}, which would make the material a good ferroelectric in the absence of free charge carriers, is the main prerequisit for the formation of large bipolarons.[29] It is interesting to note that in $Na_{24}Si_{136}$ a large displacement of Na atoms was observed already at room temperature.[30] Of course, the possibility of the formation of bipolarons in Ba_6Ge_{25} is exciting in view of the recently discovered superconductivity in this compound.[20] However, the temperature-pressure phase diagram[20] shows that, as the structural transition temperature $T_{S1,S2}$ is suppressed by increasing pressure, the superconducting transition temperature T_c is strongly enhanced. This, at first sight, seems to rule out a Bose-Einstein (BE) condensation of bipolarons[31] as a mechanism of the superconductivity in Ba_6Ge_{25}. In fact, the superconductivity in Ba_6Ge_{25} was shown[20] to be compatible with BCS theory. However, T_c of the BE condensation depends on the density n_b and the effective mass m_b of the bosons. It could also be envisioned that pressure increases n_b and/or decreases m_b leading to an enhancement of T_c.

Of course we should also consider alternative explanations for the above-described puzzle. We should ask whether any contribution to the magnetic susceptibility $\chi = \chi_{Larmor} + \chi_{struct} + \chi_e + \chi_{para}$ other than χ_e could explain the steep decrease at $T_{S1,S2}$. χ_{Larmor}, the susceptibility of the closed-shell cations, can be regarded as being temperature independent. The paramagnetic susceptibility due to local magnetic moments χ_{para} is negligibly small in the temperature range around $T_{S1,S2}$ because, here, χ is independent of the magnetic field. The only contribution which, except for χ_e, might have a pronounced temperature dependence in the range around $T_{S1,S2}$ is the structural increment χ_{struct} discussed above. The steep increase in absolute value (χ_{struct} is diamagnetic) of χ_{struct} would mean that below $T_{S1,S2}$ the molecular ring currents are enhanced, i.e., that more electrons are part of bonds with aromatic character. This is compatible with the above picture of the conduction electrons being concentrated on the Ge-cage surface between the Ba3′-Ba4 pairs. Thus, both the enhanced ring currents and the spin-singlet pairing may contribute to the sharp increase in absolute value of the magnetic susceptibility at $T_{S1,S2}$. It is interesting to note in this context that the jump of the magnetic susceptibility of C_{60} at its orientational ordering transition is discussed in terms of molecular ring currents.[32]

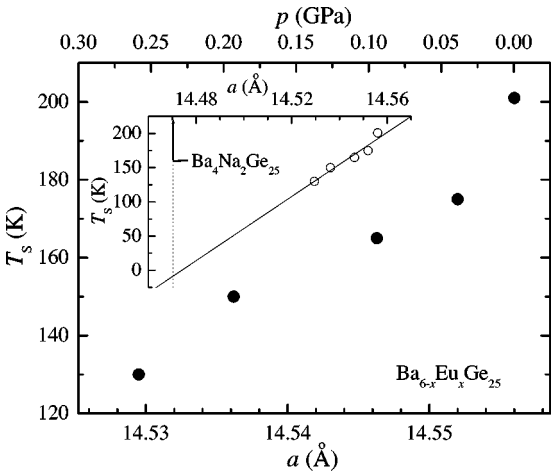

FIG. 13. Averaged transition temperature T_S for various $Ba_{6-x}Eu_xGe_{25}$ samples as a function of their lattice parameters *a*. On the upper abscissa, the pressure *p* with respect to the $x=0$ sample as determined from the bulk modulus (cf. text) is given. The inset shows the same data together with a best linear fit and its extrapolation to smaller lattice parameters.

An alternative explanation can be offered if we go beyond the free-electron picture and consider real band structure effects. In this case the conduction-electron magnetic susceptibility χ_e and the charge-carrier concentration *n* determined from the Hall-effect measurements are not directly related to each other. While χ_e is proportional to the density of states *at* the Fermi level $N(E_F)$, *n* corresponds to the integral over the density of states $N(E)$ of the conduction band up to the Fermi level E_F. A redistribution of states may conserve *n* but alter χ_e. If states are shifted from the Fermi level to below the Fermi level when cooling Ba_6Ge_{25} below $T_{S1,S2}$, χ_e would be reduced while *n* remains unchanged, just as observed in our experiments. Band structure calculations[33] indicate that such a scenario may indeed apply to Ba_6Ge_{25}.

Another origin of a reduced density of states at the Fermi level below $T_{S1,S2}$ was put foreward in Ref. 20. Assuming that the locking-in process is indeed random and that the Fermi level lies close to the band edge, a significant reduction of $N(E_F)$ will result due to the smoothing out of $N(E)$ by the high level of disorder below $T_{S1,S2}$.

Further experiments such as, e.g., nuclear magnetic resonance, optics, or electron spin resonance, will be needed to decide which of the above-discussed pictures indeed applies.

Next we discuss the suppression of $T_{S1,S2}$ upon doping Ba_6Ge_{25} with Eu, i.e., upon increasing *x* in $Ba_{6-x}Eu_xGe_{25}$. Since the two-step transition is broadened and smeared out with increasing *x*, we determined an average transition temperature T_S instead of $T_{S1,S2}$: T_S is the temperature between the first and second steps in the warming-up $\rho(T)$ curves (Fig. 2), seen as a kink in the data. In Fig. 13 we plot these temperatures T_S as a function of the lattice parameter *a*.[8] Using the bulk modulus of Ba_6Ge_{25} of approximately 48

GPa, as determined from a room-temperature x-ray diffraction study under pressure,[8] we have also calculated the pressure which corresponds to the shrinkage of the unit cell of the Eu doped samples with respect to pure Ba_6Ge_{25} and have plotted this pressure on the upper abscissa in Fig. 13. In the inset of Fig. 13 we replot the same data and show that a linear fit describes the data quite well. Assuming that this linear dependence holds down to $T_S=0$ K, the structural phase transition would be completely suppressed at $a=14.474$ Å or at $p=0.8$ GPa. This is in agreement with $Ba_4Na_2Ge_{25}$ lacking, with $a=14.4703$ Å,[7] indeed the structural phase transition. It is interesting to compare these results to pressure experiments on Ba_6Ge_{25}.[20] Below 2 GPa, $T_S=(T_{S1}+T_{S2})/2$ of Ba_6Ge_{25} decreases linearly with increasing hydrostatic pressure.[20] However, T_S of $Ba_{6-x}Eu_xGe_{25}$ decreases 5 times faster with (chemical) pressure than T_S of Ba_6Ge_{25} with (hydrostatic) pressure. In fact, according to the linear $T_S(p)$ behavior of Ba_6Ge_{25},[20] $Ba_4Na_2Ge_{25}$ should undergo a structural transition at $T_S\approx 170$ K. This indicates that doping Ba_6Ge_{25} with Eu or Na has more complex an influence than just changing the lattice parameter. Our magnetization and magnetic susceptibility measurements show that Eu is close to divalent in $Ba_{6-x}Eu_xGe_{25}$. Thus, Eu is isoelectronic with Ba. Also the size (ionic radius) and the mass of Eu are similar to the ones of Ba. Thus, the much faster suppression of T_S in $Ba_{6-x}Eu_xGe_{25}$ with increasing x than in Ba_6Ge_{25} under pressure might in some way be related to the $4f$ electrons of Eu. They appear to inhibit the locking-in of Ba (and Eu) to split sites. On the other hand, also the additional disorder introduced by the Eu doping might play an important role in suppressing T_S. In contrast to Eu, Na is not isoelectronic with Ba. Therefore, the bonding situation in $Ba_4Na_2Ge_{25}$ is different from the one in Ba_6Ge_{25}. In addition, Na is much smaller and lighter than Ba. Therefore, the absence of the structural transition in $Ba_4Na_2Ge_{25}$ can have multiple origins.

Finally we give an estimate of the bonding energy of the state which Ba_6Ge_{25} assumes below $T_{S1,S2}$, whatever its precise nature may be. The elastic energy stored, below $T_{S1,S2}$, per formula unit in Ba_6Ge_{25} may be estimated from $E_{el}=1/4\times p\Delta V=1/4\times 3pa\Delta a$. $p=2.8$ GPa is the pressure needed to remove the locking-in transition completely[20] and $\Delta a=0.011$ Å is the anomalous increase of the lattice parameter at $T_{S1,S2}$, yielding $E_{el}\approx 30$ meV.

V. SUMMARY

High-quality polycrystalline Ba_6Ge_{25} samples have been investigated by measurements of the electrical resistivity, the Hall coefficient, the magnetic susceptibility, the specific heat, the thermopower, and the thermal conductivity. A two-step phase transition of first order takes place at $T_{S1,S2}\approx 215$, 180 K, which affects all measured quantities. In Ref. 8 this phase transition was investigated in detail from the structural point of view. While the structure remains cubic, the Ba atoms in site 2 and 3 were shown to lock-in to split sites in the course of the phase transition. This structural transition strongly affects the electronic-transport properties which indicates that the phononic and electronic degrees of freedom are not decoupled in Ba_6Ge_{25}. The charge-carrier mobility is strongly reduced below the phase-transition temperature, which must be due to a strong increase of the scattering rate and/or to an increase of the effective mass of the charge carriers. An appealing scenario which accounts for the structural[8] as well as for the transport and magnetic properties is that, below $T_{S1,S2}$, the conduction electrons together with the lattice deformation build large bipolarons. However, further experiments are necessary to confirm this picture. Being a filled-cage system, Ba_6Ge_{25} is expected to be a good candidate for thermoelectric applications. The dimensionless thermoelectric figure of merit reaches 0.05 at 180 K which is comparable to the value for $Eu_8Ga_{16}Ge_{30}$.[23] While the concept of a phonon glass seems to apply to Ba_6Ge_{25}, the one of an electron crystal is heavily violated due to the strong electron-lattice interaction. We suspect that, even though Ba_6Ge_{25} is definitely an extreme example, this interaction may be important in other clathrates as well.

ACKNOWLEDGMENTS

We acknowledge useful discussions with F. M. Grosche, A. Loidl, B. Lüthi, P. Thalmeier, and I. Zerec. Part of the work was supported by the FCI (Fonds der Chemischen Industrie).

*On leave from W. Trzebiatowski Institute for Low Temperature and Structure Research, Polish Academy of Sciences, 50-950 Wroclaw, Poland.

[1] W. Carrillo-Cabrera, J. Curda, S. Paschen, and H. G. von Schnering (unpublished).
[2] W. Carrillo-Cabrera, J. Curda, H.G. von Schnering, S. Paschen, and Yu. Grin, Z. Kristallogr. **215**, 207 (2000).
[3] H. Fukuoka, K. Iwai, S. Yamanaka, H. Abe, K. Yoza, and L. Häming, J. Solid State Chem. **151**, 117 (2000).
[4] S.-J. Kim, S. Hu, C. Uher, T. Hogan, B. Huang, J.D. Corbett, and M.G. Kanatzidis, J. Solid State Chem. **153**, 321 (2000).
[5] H.G. von Schnering, R. Kröner, W. Carrillo-Cabrera, K. Peters, and R. Nesper, Z. Kristallogr. **213**, 665 (1998).
[6] H. Schäfer, Annu. Rev. Mater. Sci. **15**, 1 (1985).
[7] W. Carrillo-Cabrera, J. Curda, K. Peters, S. Paschen, Yu. Grin, and H.G. von Schnering, Z. Kristallogr. **216**, 183 (2001).
[8] W. Carrillo-Cabrera *et al.* (unpublished).
[9] G.S. Nolas, J.L. Cohn, G.A. Slack, and S.B. Schujman, Appl. Phys. Lett. **73**, 178 (1998).
[10] N.P. Blake, L. Møllnitz, G. Kresse, and H. Metiu, J. Chem. Phys. **111**, 3133 (1999).
[11] C. Uher, J. Yang, and S. Hu, in *Thermoelectric Materials 1998—The Next Generation Materials for Small Scale Refrigeration and Power Generation Applications*, edited by T. M. Tritt, H. B. Lyon, Jr., G. Maham, and M. G. Kanatzidis, Mater. Res. Soc. Symp. Proc. 545 (Materials Research Society, Pittsburgh, 1999), p. 247.
[12] G. S. Nolas, in *Thermoelectric Materials 1998* (Ref. 11), p. 435.
[13] G. A. Slack, in *CRC Handbook of Thermoelectrics*, edited by

D.M. Rowe (Chemical Rubber, Boca Raton, FL, 1995), Chap. 34.

[14] S. Paschen, V. H. Tran, M. Baenitz, W. Carrillo-Cabrera, R. Michalak, Yu. Grin, and F. Steglich, in *Proceedings of the 19th International Conference on Thermoelectrics*, edited by D. M. Rowe (Babrow Press, Wales, UK, 2000), p. 374.

[15] Due to an error in the analysis, the Hall coefficient given in Ref. 14 is too small by a factor of 2.

[16] J.B. Bieri, A. Fert, G. Creuzet, and A. Schuhl, J. Phys. F: Met. Phys. **16**, 2099 (1986).

[17] See, e.g., H. Lueken, *Magnetochemie* (B.G. Teubner, Stuttgart, 1999).

[18] C. Cros, M. Pouchard, and P. Hagenmüller, J. Solid State Chem. **2**, 570 (1970).

[19] R.C. Haddon, Nature (London) **378**, 249 (1995).

[20] F.M. Grosche, H.Q. Yuan, W. Carrillo-Cabrera, S. Paschen, C. Langhammer, F. Kromer, G. Sparn, M. Baenitz, Yu. Grin, and F. Steglich, Phys. Rev. Lett. **87**, 247003 (2001).

[21] For a review see, e.g., G.S. Nolas, G.A. Slack, and S.B. Schujman, Semicond. Semimetals **69**, 255 (2001).

[22] G.S. Nolas, T.J.R. Weakley, J.L. Cohn, and R. Sharma, Phys. Rev. B **61**, 3845 (2000).

[23] S. Paschen, W. Carrillo-Cabrera, A. Bentien, V.H. Tran, M. Baenitz, Yu. Grin, and F. Steglich, Phys. Rev. B **64**, 214404 (2001).

[24] J.L. Cohn, G.S. Nolas, V. Fessatidis, T.H. Metcalf, and G.A. Slack, Phys. Rev. Lett. **82**, 779 (1999).

[25] P.W. Anderson, Phys. Rev. Lett. **34**, 953 (1975).

[26] I. Biaggio, R.W. Hellwarth, and J.P. Partanen, Phys. Rev. Lett. **78**, 891 (1997).

[27] N. F. Mott and E. A. Davis, *Electronic processes in Non-crystalline Materials* (Clarendon Press, Oxford, 1971).

[28] D. Emin, Phys. Rev. Lett. **62**, 1544 (1989).

[29] D. Emin, Phys. Rev. B **43**, 2633 (1991).

[30] F. Brunet, P. Mélinon, A. San Miguel, P. Kéghélian, A. Perez, A.M. Flank, E. Reny, C. Cros, and M. Pouchard, Phys. Rev. B **61**, 16 550 (2000).

[31] See, e.g., N.F. Mott, Philos. Mag. Lett. **63**, 319 (1991).

[32] A.P. Ramirez, R.C. Haddon, O. Zhou, R.M. Fleming, J. Zhang, S.M. McClure, and R.E. Smalley, Science **265**, 84 (1994).

[33] I. Zerec, A. Yaresko, P. Thalmeier, and Yu. Grin (unpublished).